Nano Research

Open Access

Research Article

Protein-based functional hydrogel improves cutaneous nerve repair and diabetic wound healing

Hanzhi Lu[1,§], Mingrui Cui[2,§], Yi Wang[1,§], Xinran Du[1], Xinyi Zhou[1], Yuhan Fang[1], Xiaoyan Gao[1], Ying Peng[3], Jianyong Zhu[3], Guang Yang[2] ✉, and Fulun Li[1] ✉

[1] *Department of Dermatology, Yueyang Hospital of Integrated Traditional Chinese and Western Medicine, Shanghai University of Traditional Chinese Medicine, Shanghai 200437, China*
[2] *Shanghai Engineering Research Center of Nano-Biomaterials and Regenerative Medicine, College of Biological Science and Medical Engineering, Donghua University, Shanghai 201620, China*
[3] *Clinical Laboratory Medicine Center, Yueyang Hospital of Integrated Traditional Chinese and Western Medicine, Shanghai University of Traditional Chinese Medicine, Shanghai 200437, China*
§ *Hanzhi Lu, Mingrui Cui, and Yi Wang contributed equally to this work.*

Cite this article: *Nano Research*, **2025**, *18*, 94907012. https://doi.org/10.26599/NR.2025.94907012

ABSTRACT: Cutaneous nerve regeneration in diabetic wounds remains a challenge for current clinical treatment. Herein, a natural protein-based functional hydrogel is developed using keratin as the sole matrix, and protocatechuic aldehyde (PA) and zinc ions as the building blocks through dual-dynamic crosslinking reactions of thiol-aldehyde addition and catechol-zinc ions coordination. The unique structural design endows the hydrogel with excellent injectability, skin adhesion, self-healing and antibacterial ability, and biocompatibility. In addition, this hydrogel acts as a drug carrier for the loading and sustained release of phellopterin (PP), a natural compound extracted from traditional Chinese medicine *Angelica dahurica*. Our findings demonstrate that the PP-loaded hydrogel promotes cutaneous nerve regeneration, angiogenesis and tissue remodeling in the full-thickness wounds in both db/db and streptozotocin-induced C57BL/6 diabetic mice, notably by the synergistic effect of zinc ions and PP, showing a great potential in diabetic wound therapy.

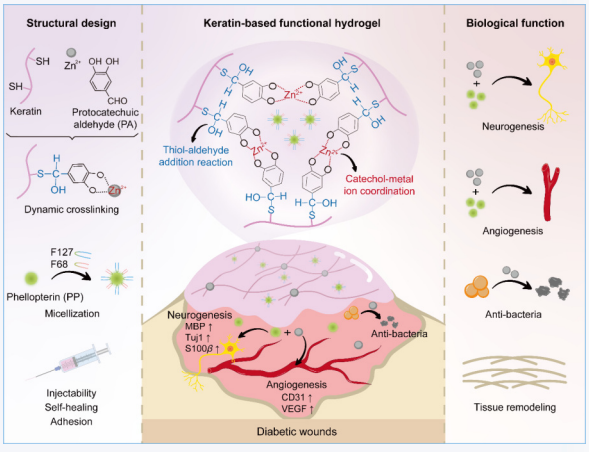

KEYWORDS: functional hydrogel, cutaneous nerve regeneration, dynamic crosslinking, diabetic wounds

1 Introduction

Diabetic wounds are major complications of diabetes and are associated with increasing incidence, high morbidity, and socioeconomic burden [1]. Clinical studies have shown that peripheral neuropathy, inflammatory dysfunction, reduced angiogenesis and uncontrolled bacterial infection are involved in the pathogenesis of diabetic wounds and lead to an impaired or even nonhealing state [2–4]. Therefore, there is an urgent need to develop comprehensive treatment strategies due to the complexity of diabetic wounds.

Received: July 5, 2024; **Revised:** August 22, 2024
Accepted: August 28, 2024

✉Address correspondence to Guang Yang, gyang@dhu.edu.cn; Fulun Li, drlifulun@163.com

Wound dressings hold great promise in the management of diabetic wounds, among which hydrogels are considered desirable dressings because of their good biocompatibility and robust delivery ability [5]. However, traditional hydrogel dressings have several limitations, such as incomplete filling of irregular wound beds, confinement of joint movement, and a lack of antibacterial function. In this context, hydrogel dressings with desirable adhesive, mechanical, and antibacterial abilities are good candidates for the clinical treatment of diabetic wounds [6]. However, complex synthesis procedures are often required for the development of functional hydrogels, especially those derived from natural polymers, owing to their limited active chemical groups, which in turn compromise the inherent biocompatibility of hydrogel dressings.

To achieve superior treatment outcomes, various therapeutics, including endogenous cells, extracellular vesicles, therapeutic nanoparticles, and chemical drugs, are loaded in hydrogels to

endow dressings with anti-inflammatory, angiogenic, or epithelialization functions [7–11]. Despite the promotion of wound closure by current therapeutic strategies, the restoration of nerve function is often overlooked, which has the potential to limit the quality of life and long-term prognosis of patients [12]. Tissue injury is frequently accompanied by nerve damage, particularly in chronic wounds such as diabetic ulcers. Neurodegenerative changes can significantly impact the healing process and functional recovery of the skin, leading to sensory loss and motor dysfunction [13]. However, the development of wound dressings with cutaneous nerve regeneration is still in its infancy owing to the current lack of innervation-related therapies or material design methods [14].

In this work, we developed a protein-based therapeutic hydrogel for cutaneous nerve regeneration and diabetic wound healing (Fig. 1). For this hydrogel, keratin is used as the sole matrix, and naturally derived chemicals, protocatechuic aldehyde (PA) and zinc ions, are used as building blocks to form dynamic chemical crosslinks with keratin in a mild and simple fashion. Keratin is a type of cysteine-rich natural protein that widely exists in skin and skin appendages such as hair and wool [15]. Emerging evidence shows that keratin possesses good biocompatibility and wound repair ability [16]. Notably, the inherent free thiol groups in keratin serve as active groups for exploring functional hydrogels [16]. Zinc ions have been reported to stimulate nerve regeneration and angiogenesis during the wound healing process [17]. PA is derived from the Chinese herb *Salvia miltiorrhiza* and has an aldehyde group and a catechol group in its chemical structure [18]. The unique chemical structure allows PA to form catechol–metal ion coordination bonds with zinc ions and dynamic crosslinking with keratin through an aldehyde–thiol addition reaction. The preparation process of the hydrogel needs only physical mixing under mild conditions, without the involvement of extra catalysts, crosslinkers, or chemical modification of keratin. In addition, phellopterin (PP), a natural compound extracted from the traditional Chinese medicine *Angelica dahurica*, is encapsulated in F127/F68 mixed micelles and loaded into the hydrogel. The effects of PP and the PP-loaded hydrogel on nerve regeneration were investigated *in vitro*, and their effects on the healing of full-thickness wounds in both db/db and streptozotocin-induced C57BL/6 diabetic mice were evaluated.

2 Experimental

2.1 Preparation of phellopterin-loaded ker-PA/Zn hydrogels

The PA/Zn complex was prepared according to the literature [19, 20]. PA was dissolved in 80 °C deionized water and then combined with zinc acetate solution at a PA:Zn molar ratio of 2:1. The pH value of the solution was adjusted to 10.0 with ammonium hydroxide. The PA/Zn complex was obtained after stirring at room temperature for 12 h and analyzed via an ultraviolet–visible (UV–vis) spectrophotometer. An 18% w/v keratin solution was prepared by dissolving 0.09 g of keratin in 0.5 mL of deionized water. The PA/Zn complex mixture was mixed with the keratin mixture, and the final PA concentration in the hydrogel was adjusted to 0.1%, 0.2%, or 0.3% w/v. The mixture was stirred for several seconds and then placed statically to form a hydrogel. The obtained hydrogels were denoted as ker-PA/Zn 0.1, ker-PA/Zn 0.2, and ker-PA/Zn 0.3, respectively. PP was loaded in F127/F68 mixed micelles to increase water solubility via a thin-film hydration method according to the literature [21, 22]. The PP-loaded hydrogel was fabricated by mixing 200 μL of the PP micelles with 800 μL of the hydrogel precursor solution at a PA concentration of 0.2% and then placing them statically to form a hydrogel. The final concentration of PP in the ker-PA/Zn 0.2 hydrogel was 2 μg/mL, and the resulting hydrogel was recorded as the ker-PA/Zn/PP 0.2 hydrogel.

2.2 *In vivo* evaluation of diabetic wound healing

The animal experiments were approved by the Animal Care and

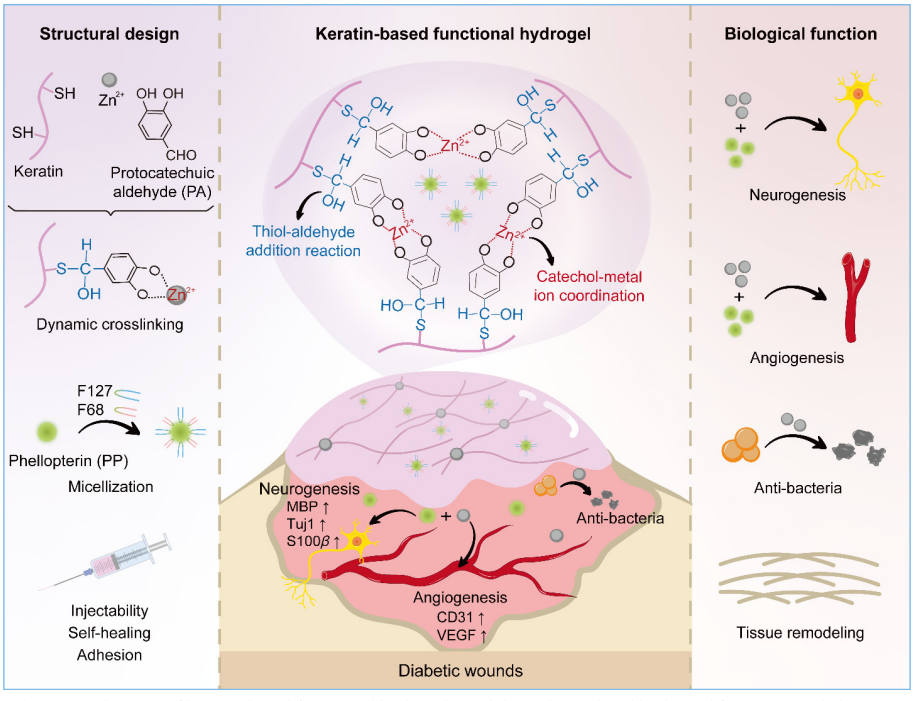

Figure 1 Schematic of the gelation mechanism of keratin-based functional hydrogels, and their physical and biological functions in diabetic wound healing.

Use Committee of Yueyang Hospital of Integrated Traditional Chinese and Western Medicine affiliated with Shanghai University of Traditional Chinese Medicine. Male db/db mice (8–10 weeks old) and C57BL/6J mice (6–8 weeks old) were procured from Shanghai SLAC Laboratory Animal Co., Ltd. C57BL/6J mice were first fed high-fat feed for 3 weeks and then received daily intraperitoneal injections of low-dose streptozotocin (STZ) solution (50 mg/kg STZ dissolved in 0.5 mol/L, pH 4.5 sodium citrate buffer) for 7 days to induce type 1 diabetes. Mice with a blood glucose level exceeding 16.7 mmol/L one week after the last STZ injection were considered diabetic. After disinfection with 75% alcohol, a full-thickness circular wound approximately 6 mm in diameter was created on the dorsal area via surgical scissors. The wounds were grouped and topically treated with sterilized PBS solution, ker-PA/Zn 0.2 hydrogel, ker-PA/Zn/PP 0.2 hydrogel, or recombinant bovine basic fibroblast growth factor (rb-bFGF, Zhuhai Yisheng Biological Pharmaceutical, Zhuhai, China). The hydrogels or rb-bFGF were changed every 2 days. The wounds were recorded on days 0, 2, 4, 6, and 9. The wound areas were measured with ImageJ software, and the wound healing rates were calculated based on the wound areas [16].

3 Results and discussion

3.1 Preparation and evaluation of ker-PA/Zn hydrogels

The ker-PA/Zn hydrogel was prepared by simple mixing of 18% keratin solution and a PA/Zn complex solution at room temperature. The PA/Zn complex was formed through dynamic crosslinking between Zn ions and the catechol groups in PA, which was confirmed by the UV–vis absorption spectrum (Fig. 2(a)). PA displayed two absorption peaks at 278 and 313 nm, which were attributed to the presence of an aromatic ring connected to two phenolic hydroxyls and one carbonyl group. For the PA/Zn complex, an obvious peak at 344 nm appeared in the spectrum due to a redshift in the absorption peak of the PA molecule resulting from Zn^{2+} coordination [23]. The PA/Zn complex and keratin formed a hydrogel through a reversible thiol–aldehyde addition

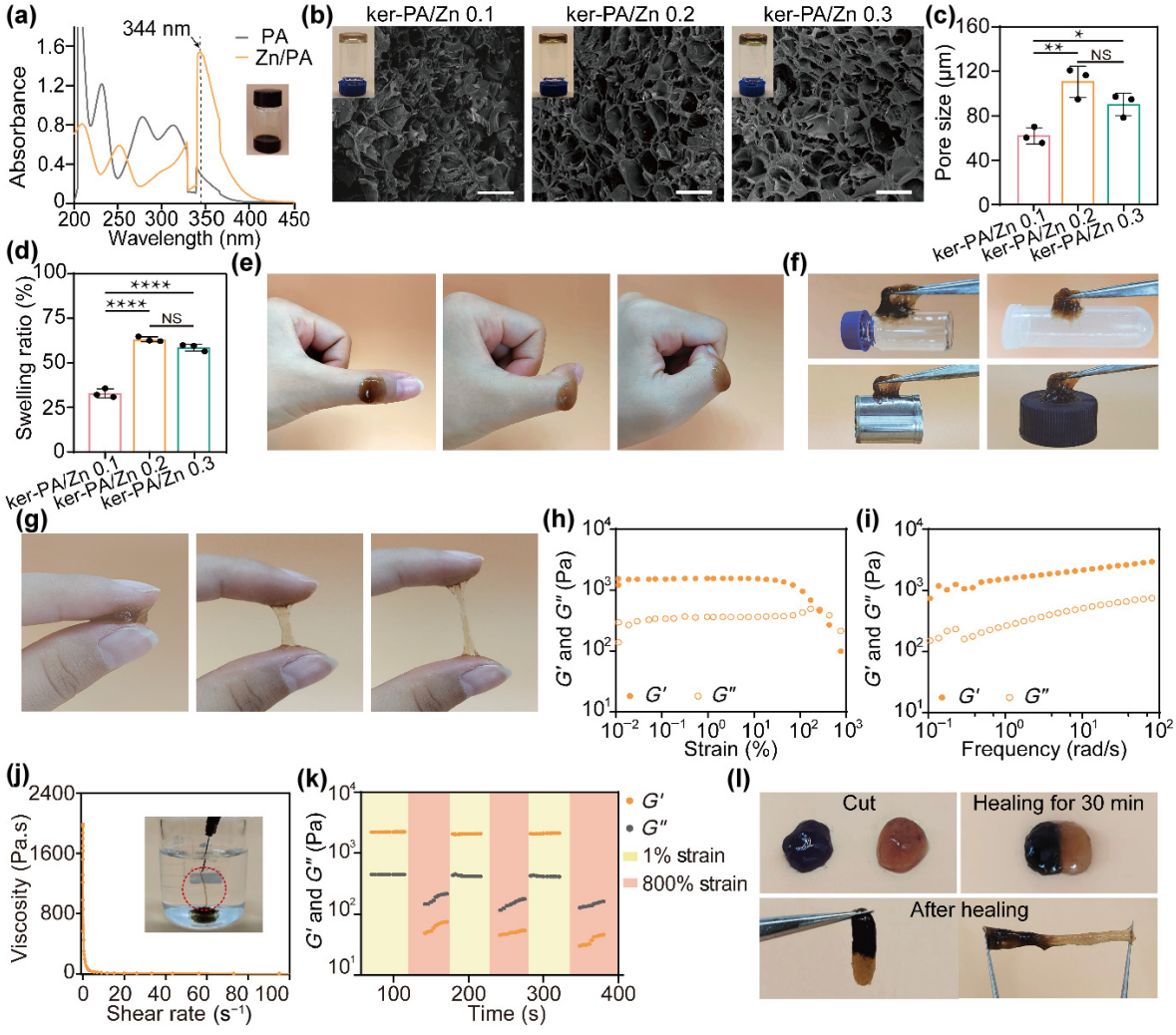

Figure 2 Preparation and evaluation of ker-PA/Zn hydrogels. (a) UV–vis spectra of PA and the PA/Zn complex and a photograph of the PA/Zn complex solution. (b) Digital images and SEM images of ker-PA/Zn hydrogels. Scale bars: 200 μm. (c) Average pore sizes measured from SEM images. (d) Equilibrium swelling ratios of the ker-PA/Zn hydrogels. (e) Pictures of the hydrogel adhered to the bending finger joint. (f) Pictures of the hydrogels adhered to various materials. (g) Pictures of the hydrogel compressed and stretched by fingers. (h) Strain sweeps of the ker-PA/Zn 0.2 hydrogel. (i) Rheological properties of the ker-PA/Zn 0.2 hydrogel. (j) Shear-thinning test of the hydrogel and image of the hydrogel injected through a 26-gauge syringe needle into water. (k) Rheological behavior of the hydrogel with alternate strain cycles. (l) Pictures of the self-healing ability of the hydrogel. The data are represented as the means ± SDs. NS indicates no significant differences; $^{*}P < 0.05$, $^{**}P < 0.01$ and $^{****}P < 0.0001$.

reaction between the thiol groups in keratin and the aldehyde groups in PA [24]. Figure 2(b) shows digital images and SEM images of the ker-PA/Zn hydrogels with a keratin concentration of 18% w/v and PA/Zn complex concentrations of 0.1%, 0.2% and 0.3% w/v. All hydrogels had a porous microstructure with an average pore size of ~ 60–110 μm (Fig. 2(c)). The swelling ratios of the hydrogels had a similar trend as the pore size. A greater pore size resulted in an increased swelling ratio of the hydrogel (2(d)).

Figures 2(e) and 2(f) show that the ker-PA/Zn hydrogel had good adhesion ability; it can adhere to the bending finger joint without falling off, as well as other materials such as glass, plastic and metal, mainly because of the existence of the catechol and aldehyde groups in PA. The dynamic crosslinked structure endows the hydrogel with good elasticity, injectability, and self-healing properties. Figure 2(g) shows that the hydrogel underwent compression and stretching between fingers. After being compressed by fingers, the hydrogel could be stretched to more than 5 times the original height without obvious breakage, implying good elasticity. Rheological tests were performed to investigate the rheological properties of the hydrogels. The linear viscoelastic region of the hydrogels was determined, and 1% strain was chosen for further rheological tests (Fig. 2(h)). Figure 2(i) shows that the storage modulus (G') of the hydrogel was greater than the loss modulus (G'') at every frequency, verifying that the ker-PA/Zn hydrogel had elastic properties. The shear-thinning property of the hydrogel was also investigated via rheological tests (Fig. 2(j)). The viscosity decreased sharply with increasing shear rate, indicating that the hydrogel had obvious shear-thinning behavior. This endows the hydrogel with outstanding injectability. The inserted picture in Fig. 2(j) shows that the hydrogel could be easily injected into water through a 26-gauge syringe needle. The continuous cyclic strain test demonstrated that at a high strain of 800%, the G' value of the hydrogel decreased from ~ 2000 to ~ 60 Pa and was lower than G'', implying the collapse of the hydrogel network. When the strain decreased to 1%, the G' value almost returned to its initial value, implying recovery of the hydrogel network. This collapse and recovery of the hydrogel network could be repeated for at least three cycles (Fig. 2(k)). This result indicated that the hydrogel had good self-healing capacity, which was further confirmed by a macroscopic healing test (Fig. 2(l)). Two parts of the hydrogel disk could be rejoined after contact for 30 min and maintained integrity when it was stretched after healing. These results demonstrated that the Ker-PA/Zn hydrogel had excellent injectability, tissue adhesion and self-healing properties, potentially satisfying the practical applications of the hydrogel as a wound dressing.

3.2 Drug release, antibacterial ability and biocompatibility

F127/F68 mixed micelles were used to encapsulate PP for improved water solubility and were loaded into the hydrogel with a drug loading content of 2 μg/mL. The release profile revealed that the cumulative release of PP reached approximately 36% after 48 h of incubation in normal saline at 37 °C (Fig. 3(a)). The hemolysis test demonstrated that the hydrogels at PA/Zn complex concentrations of 0.1%–0.3% did not induce apparent hemolysis, with hemolysis ratios less than 5% (Fig. 3(b)). Owing to the presence of zinc ions, the ker-PA/Zn hydrogel exhibited significant antibacterial ability against *S. aureus*, as reflected by both the inhibition zone and colony counting tests. As shown in Fig. 3(c), the hydrogels at three PA/Zn complex concentrations displayed obvious inhibition zones after incubation for 24 h, and those at a higher PA/Zn complex concentration presented a larger inhibition zone. Colony counting assays were used to quantitatively test the antibacterial ability of the hydrogels (Fig. 3(d)). The hydrogels at three PA/Zn complex concentrations achieved a high antibacterial rate of close to 100% (Fig. 3(e)). Moreover, the PP-loaded hydrogels presented similar results in terms of both the inhibition zones and antibacterial rates to the hydrogels (data not shown), indicating that PP had no antibacterial activity. The cytotoxicity of the ker-PA/Zn hydrogel was evaluated by both a cell viability assay and a live/dead assay using L929 mouse fibroblasts. Compared with the PBS group, the hydrogels treated with the three PA/Zn complexes and the PP-loaded hydrogel had no significant differences in terms of cell proliferation at 1, 3 and 5 days of incubation (Fig. 3(f)). The live/dead staining assay confirmed that the number of live cells increased over time of incubation, whereas few dead cells were observed during incubation (Fig. 3(g)). Considering its antimicrobial properties and biosafety profile, the ker-PA/Zn 0.2 hydrogel was selected for subsequent experiments.

3.3 *In vitro* migration and remyelination evaluation of RSC96 cells

The innervation process is essential for high-quality wound repair [25–27]. Studies have shown that mature Schwann cells can form lamellipodia to facilitate axon extension [28–32]. They also participate in domain differentiation and provide local structural and metabolic support for nerve regeneration and repair [33]. In this work, a cell scratch test was performed to assess the effects of ker-PA/Zn 0.2 hydrogel, PP-loaded hydrogel (ker-PA/Zn/PP 0.2) and PP solution (same concentration of 2 μg/mL, without encapsulation in F127/F68 micelles) on Schwann cell migration in normal glucose and high glucose environments (Figs. 4(a) and 4(b)). The cells without any treatment were used as a control. Under normal glucose conditions, compared with those in the control group, both the ker-PA/Zn 0.2 and PP solutions significantly facilitated cell migration and the formation of lamellipodia (Fig. 4(c)). In particular, ker-PA/Zn/PP 0.2 promoted the complete movement of the cells at the center after incubation for 24 h. A cell migration assay of Schwann cells exposed to high glucose was further performed to evaluate the protective effects of the hydrogels. Compared with that of the control group without glucose, the cell migration ability was lower in the high-glucose environment. In contrast, both the ker-PA/Zn 0.2 and PP solutions resisted the inhibitory effect of glucose, and the ker-PA/Zn/PP 0.2 solution was superior to either solution alone (Fig. 4(d)).

According to the literature, S100β is a typical Schwann cell cytoplasmic marker protein that plays a pivotal role in neural axon growth, cell signaling, movement, and metabolism [34]. The Tuj1 protein is a marker of axonal regeneration [35]. Phalloidin is used as a staining agent for the actin cytoskeleton, allowing for the investigation of cellular morphology and migratory behavior [36]. The effects of ker-PA/Zn/PP 0.2 on glial expression in Schwann cells were studied via immunofluorescence staining of neural-specific proteins, including a Schwann cell surface marker (S100β) and a myelin regeneration marker (Tuj1). The ker-PA/Zn 0.2 hydrogel and PP solution were set for comparison. In contrast to those in the control group, the expression levels of both protein markers were increased in all three groups, among which the ker-PA/Zn/PP 0.2 group presented significantly greater levels than the ker-PA/Zn 0.2 and PP solutions did (Figs. 4(e) and 4(f)). Furthermore, the cells in the ker-PA/Zn/PP 0.2 group exhibited a

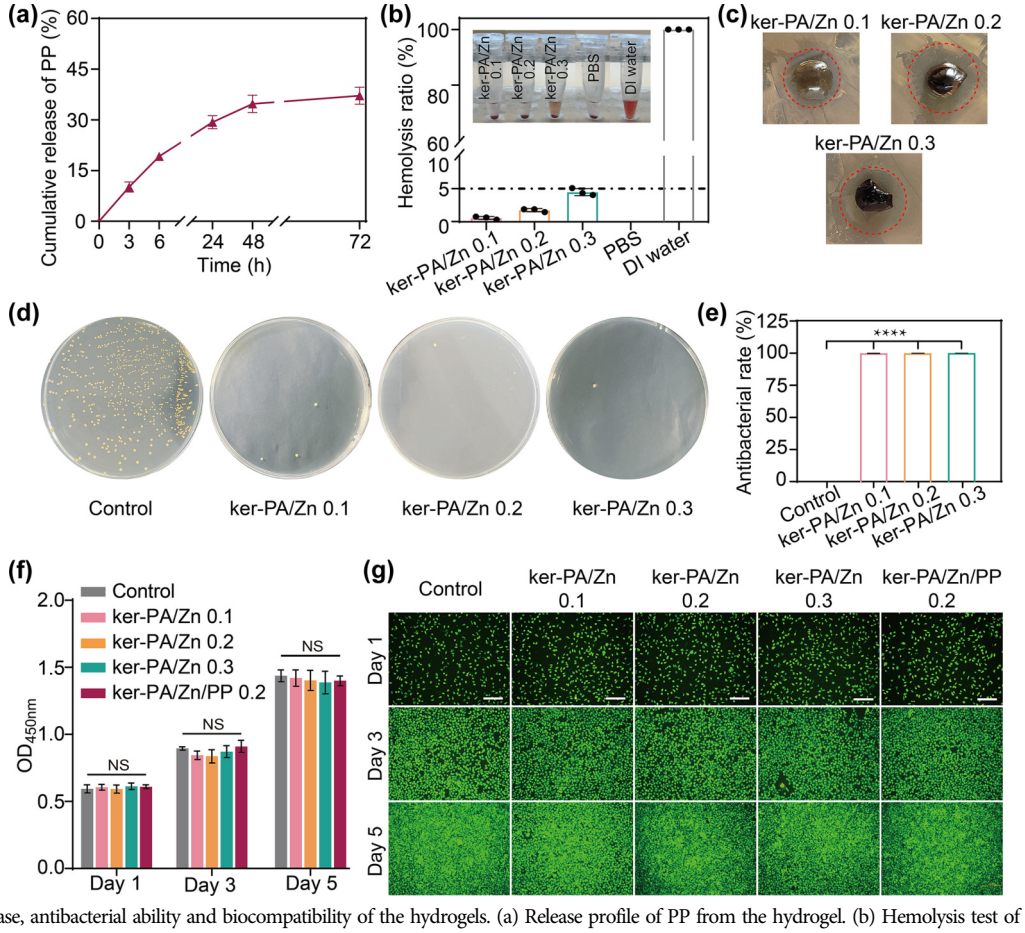

Figure 3 Drug release, antibacterial ability and biocompatibility of the hydrogels. (a) Release profile of PP from the hydrogel. (b) Hemolysis test of the hydrogels. PBS and deionized (DI) water were used as negative and positive controls, respectively. (c) Assessment of antibacterial activity against *S. aureus* via the inhibition zone method. (d) Pictures of bacterial colonies on agar plates after contact with the hydrogels at three PA/Zn complex concentrations, with PBS as a control. (e) Bacterial viability of the hydrogels based on Fig. 2(d). (f) Cell viability of L929 mouse fibroblasts after 1, 3 and 5 days of incubation. (g) Live/dead staining of L929 mouse fibroblasts after 1, 3 and 5 days of incubation. Scale bar: 200 μm. The data are presented as the means ± SDs. NS indicates not significant, and ****$P < 0.0001$.

more extended and elongated state, with the formation of distinct lamellipodia (Fig. 4(f), marked with white arrows). The morphology of the Schwann cells was further observed by staining the actin cytoskeleton with phalloidin (Fig. 4(g)). The cells in the ker-PA/Zn/PP 0.2 group exhibited more elongated protrusions (lamellipodia) than those in the ker-PA/Zn 0.2 and PP groups did. These results indicated that both ker-PA/Zn 0.2 and PP could facilitate Schwann cell migration under normal and even high-glucose conditions and that ker-PA/Zn/PP 0.2 could achieve a superior effect because of the synergistic action of ker-PA/Zn 0.2 and PP.

3.4 Diabetic wound healing test

A full-thickness diabetic wound model (~ 6 mm in diameter) in both db/db mice and STZ-induced C57BL/6 mice was used to evaluate the therapeutic efficacy of the ker-PA/Zn 0.2 and ker-PA/Zn/PP 0.2 hydrogels (Fig. 5(a)). Wounds treated with PBS were used as controls, and rb-bFGF was applied for comparison. Representative images of the wounds in all the groups on days 0, 2, 4, 6, and 9 after injury are shown in Fig. 5(b), and the corresponding quantitative wound healing rates were calculated from these images (Figs. 5(c) and 5(d)). For both the db/db mice and the STZ-induced C57BL/6 mice, the ker-PA/Zn 0.2 hydrogel resulted in faster wound closure than did the control after 2 days, with healing rates reaching 87.7% for the db/db mice and 72.5% for the C57BL/6 mice. In contrast, the wound healing rates in the control group were only 71.4% and 60.8%, respectively, on day 9. Notably, the PP-loaded hydrogel further accelerated wound closure, resulting in a similar healing rate to that of the rb-bFGF group for db/db mice (94.0% vs. 96.2%) on day 9 and an even higher healing rate than that of the rb-bFGF group (90.5% vs. 73.8%) for C57BL/6 mice.

3.5 Epidermal and dermal remodeling in diabetic wounds

Re-epithelialization is crucial for reestablishing the epidermal barrier during the wound healing process. In this work, the re-epithelialization of wounds in each group was assessed on day 4 via hematoxylin and eosin (H&E) staining (Fig. 6(a)). The results revealed that the epidermal migration length in the ker-PA/Zn/PP 0.2 group was greater than that in the control, ker-PA/Zn 0.2 and rb-bFGF groups on day 4 (Fig. 6(b)). The re-epithelialization process further accelerated wound healing, with the ker-PA/Zn/PP 0.2 group having the smallest wound width on day 9 among all the groups (Fig. 6(c)).

Collagen deposition and tissue remodeling also play important roles in restoring the tensile strength of the tissue at the wound site [37]. Masson staining was conducted on days 4 and 9 to evaluate collagen deposition and tissue remodeling in every group (Fig. 6(d)). Compared with the control, both ker-PA/Zn/PP 0.2 and ker-PA/Zn 0.2 promoted collagen deposition, and ker-PA/Zn/PP

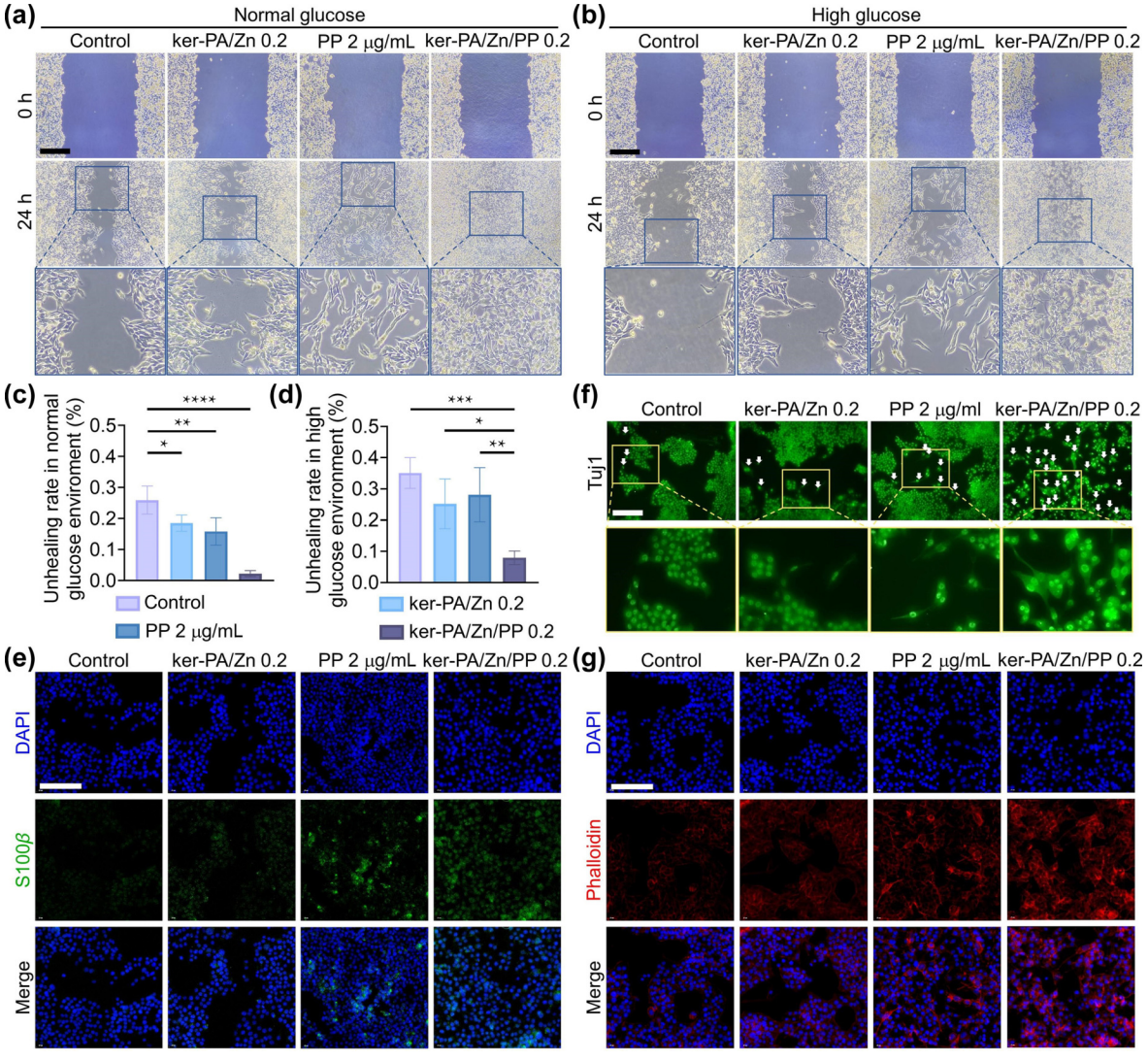

Figure 4 *In vitro* migration and remyelination evaluation. (a) Cell migration assay of Schwann cells in a normal glucose environment. Scale bars: 100 μm. (b) Cell migration assay of Schwann cells in a high-glucose environment. Scale bars: 100 μm. (c) Quantification of cell migration based on (a). (d) Quantification of cell migration based on (b). Immunofluorescence staining of (e) S100*β*, (f) Tuj1, and (g) phalloidin in Schwann cells. Scale bars: 100 μm. The data are presented as the means ± SDs. NS means not significant; $^{*}P < 0.05$, $^{**}P < 0.01$, and $^{***}P < 0.001$.

0.2 achieved a better effect than rb-bFGF did (Fig. 6(e)). Additionally, compared with rb-bFGF, both ker-PA/Zn/PP 0.2 and ker-PA/Zn 0.2 stimulated the regeneration of dermal appendages on day 9 (Fig. 6(f)). This result was consistent with other studies showing that both zinc ions and keratin could facilitate hair follicle regeneration [38, 39].

3.6 Cutaneous nerve repair in diabetic wounds

The impact of ker-PA/Zn/PP 0.2 on glial expression in Schwann cells was investigated *in vivo* via immunohistochemical staining of a myelin regeneration marker (Tuj1), a Schwann cell surface marker (S100*β*) and a neural fiber myelination marker (MBP) (Fig. 7(a)) [40]. In contrast to the control, both ker-PA/Zn 0.2 and ker-PA/Zn/PP 0.2 resulted in greater expression of Tuj1, S100β and MBP on days 4 and 9, respectively, especially for the ker-PA/Zn/PP 0.2 hydrogel (Figs. 7(b)–7(d)).

Studies have shown that diabetic wounds are characterized by a decreased distribution of growth-associated protein 43 (GAP43)-labeled axons [41, 42] and the loss of protein-encoding gene product 9.5 (PGP9.5)-labeled axons [43]. The effect of the ker-PA/Zn/PP 0.2 hydrogel on nerve axon regeneration was assessed via immunohistochemical staining of the axonal markers GAP43 and PGP9.5 (Fig. 8(a)). The results demonstrated that the ker-PA/Zn 0.2 hydrogel resulted in greater expression of GAP43 and PGP9.5 than the control on days 4 and 9 (Figs. 8(b) and 8(c)). Moreover, the ker-PA/Zn/PP 0.2 hydrogel further increased the expression of GAP43 and PGP9.5 compared with the ker-PA/Zn 0.2 hydrogel, with values greater than or similar to those in the rb-bFGF group. These results indicated that the ker-PA/Zn/PP 0.2 hydrogel promoted the regeneration of damaged nerves, largely because of its role in the activation, migration, and myelination of Schwann cells [17, 44].

3.7 Neoangiogenesis in diabetic wounds

Neoangiogenesis plays a key role in transporting nutrients and oxygen to wounds during the proliferative phase, thus facilitating fibroblast proliferation, collagen synthesis, re-epithelialization and neurogenesis [45, 46]. The effect of the hydrogels on

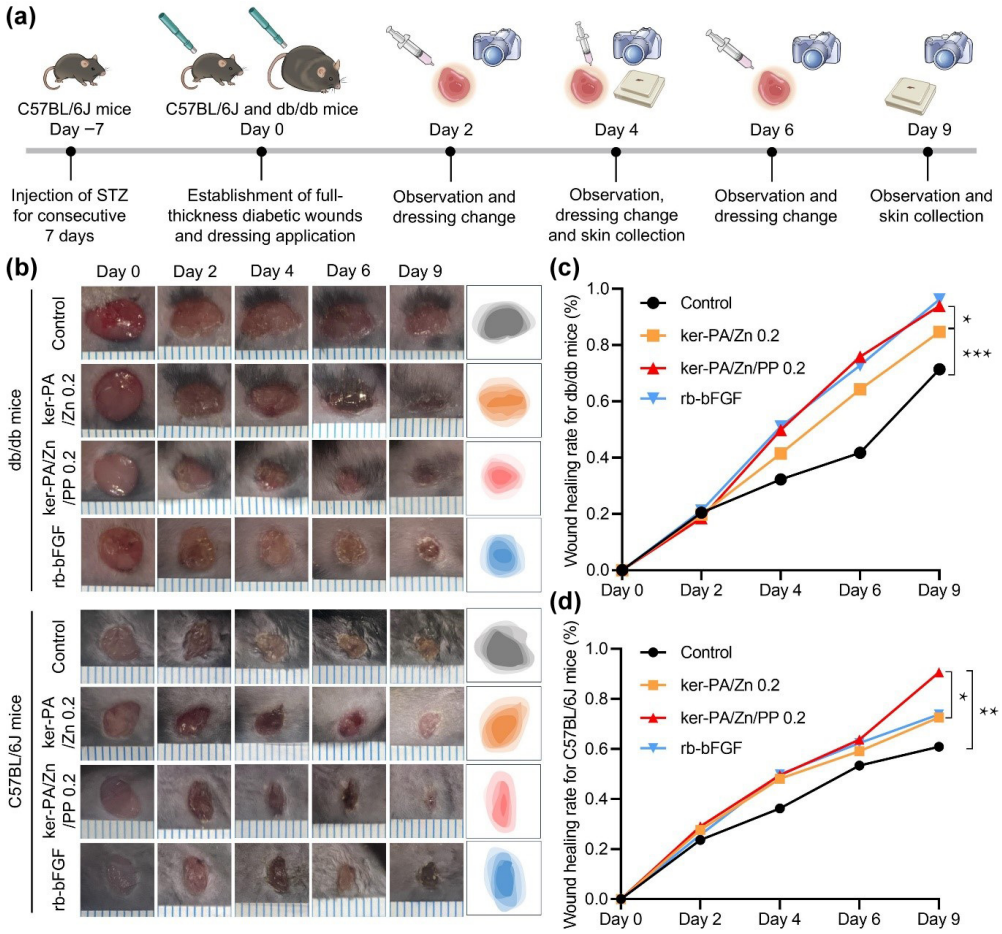

Figure 5 *In vivo* evaluation of the effects of ker-PA/Zn 0.2 and ker-PA/Zn/PP 0.2 hydrogels on diabetic wound healing in both db/db mice and STZ-induced C57BL/6 mice. Wounds treated with PBS were used as controls, and rb-bFGF was used for comparison. (a) Schematic of the experimental timeline for the wound healing test. (b) Representative images of the wounds in all groups on days 0, 2, 4, 6, and 9 after injury. (c) Quantitative analysis of the wound healing rates of db/db mice (n = 5). (d) Quantitative analysis of the wound healing rates of STZ-induced C57BL/6 mice (n = 5). *P < 0.05, **P < 0.01 and ***P < 0.001.

neoangiogenesis was evaluated through immunohistochemical staining of platelet endothelial cell adhesion molecule-1 (CD31) and vascular endothelial growth factor (VEGF) in granulation tissue (Fig. 9(a)). Compared with the control, ker-PA/Zn 0.2 increased the expression of CD31 and VEGF on days 4 and 9, indicating that zinc ions play a role in angiogenesis. Moreover, ker-PA/Zn/PP 0.2 resulted in the highest expression of CD31 and VEGF on day 4 among all the groups (Figs. 9(b) and 9(c)), demonstrating that mixed micelles of PP could facilitate angiogenesis. According to the literature, neoangiogenesis can stimulate axon regeneration in axon-deficient chronic diabetic ulcers by supporting the elevated metabolic demands of nerve cells, thus accelerating wound healing [46].

4 Conclusions

In this work, we describe a protein-based functional hydrogel with injectability, skin adhesion, self-healing and antibacterial ability for diabetic wound repair. A mixture of micelles of phellopterin, a natural compound extracted from the traditional Chinese medicine *Angelica dahurica*, was demonstrated for the first time as a therapeutic for accelerating cutaneous nerve regeneration and angiogenesis in full-thickness diabetic wounds. Additionally, the phellopterin-loaded hydrogel achieved better treatment outcomes in diabetic wound healing than rb-bFGF did because of the synergistic effect of phellopterin and zinc ions. These results demonstrated that the phellopterin-loaded hydrogel could serve as a desirable hydrogel dressing for diabetic wound treatment.

Electronic Supplementary Material: Supplementary material (further details of the synthesis processes and methods for evaluating the properties of the hydrogel) is available in the online version of this article at https://doi.org/10.26599/NR.2025.94907012.

Data availability

Not applicable.

Acknowledgements

This work was supported by grants from the National Natural Science Foundation of China (Nos. 82474515 and 82074428), High-level Chinese Medicine Key Discipline Construction Project (Integrative Chinese and Western Medicine Clinic) of National Administration of TCM (No. zyyzdxk-2023065), Young Qi-Huang Scholar of National Administration of Traditional Chinese Medicine, Evidence-Based Capacity Building for TCM Specialty Therapies for Skin Diseases of National Administration of TCM, and Innovative Team Projects of Shanghai Municipal Commission

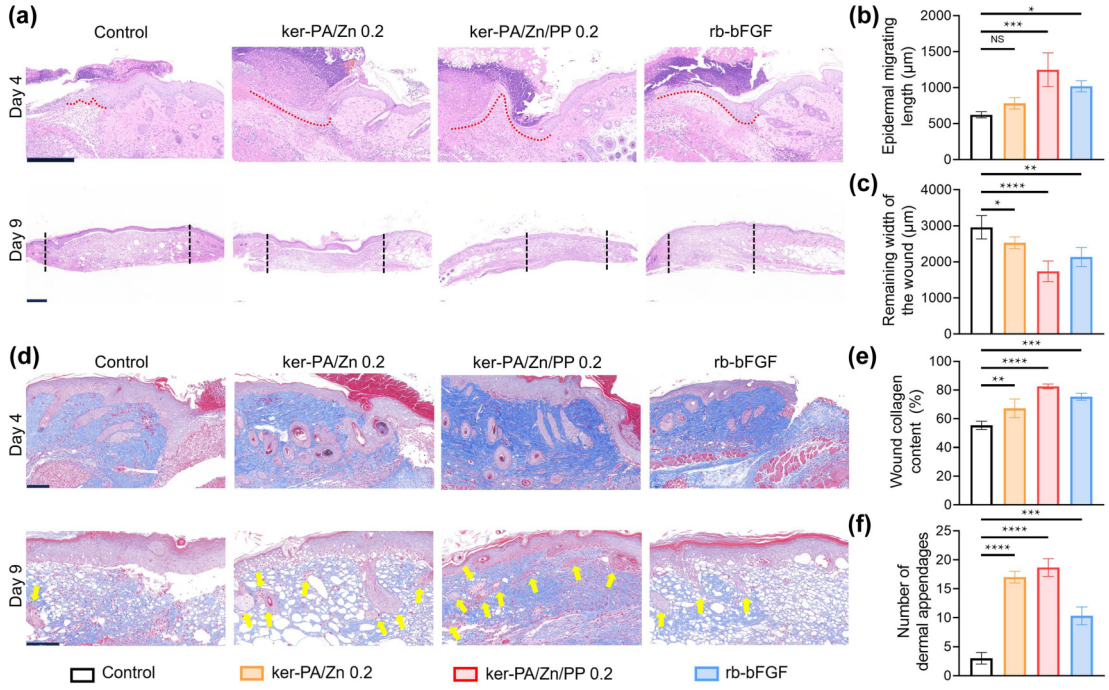

Figure 6 *In vivo* evaluation of collagen deposition and tissue remodeling of ker-PA/Zn 0.2 and ker-PA/Zn/PP 0.2 hydrogels in diabetic wounds. (a) H&E staining of wounds on days 4 and 9 postinjury. Scale bars: 300 μm. The red dotted lines outline the migration of epithelial tongues; the black dotted lines mark the edges of the wounds. (b) Quantitative assessment of epidermal migration length on day 4 based on (a). (c) Quantitative measurement of the remaining width of the wound on day 9 according to (a). (d) Masson staining of the wounds on days 4 and 9 postinjury. Scale bars: 100 μm. The yellow arrows indicate new dermal appendages on day 9. (e) Quantitative assessment of collagen density on day 4. (f) Quantification of the number of dermal appendages on day 9. The data are presented as the means ± SDs. NS means not significant; $^{*}P < 0.05$, $^{**}P < 0.01$, $^{***}P < 0.001$, and $^{****}P < 0.0001$.

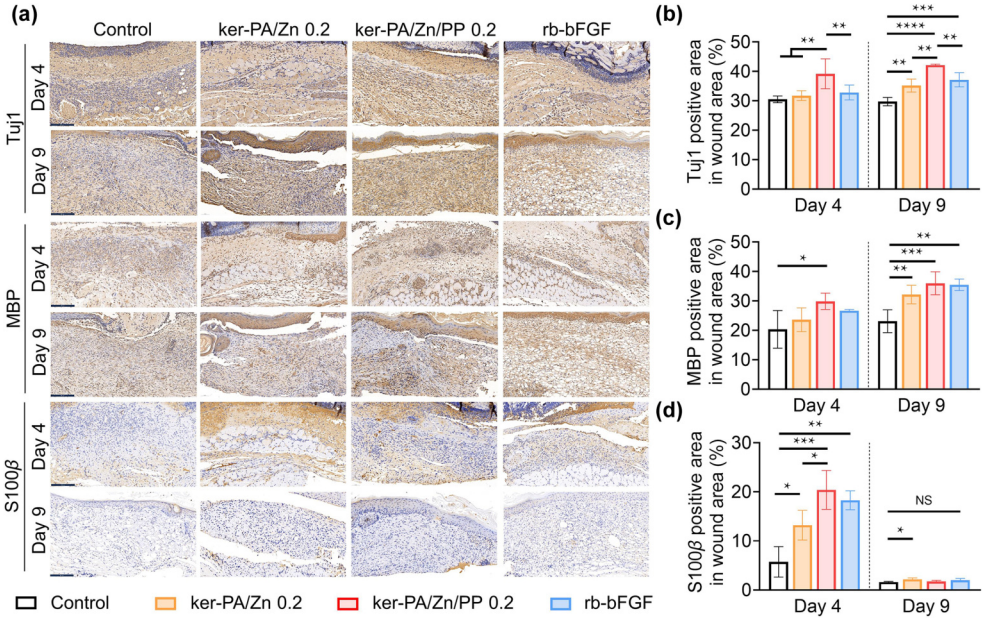

Figure 7 Effect of the ker-PA/Zn/PP 0.2 hydrogel on Schwann cell maturation in diabetic wounds. (a) Immunohistochemical staining of glia and neuroproteins (Tuj1, MBP and S100*β*) ($n = 3$). Scale bars: 150 μm. Quantitative analysis of (b) Tuj1, (c) MBP and (d) S100*β* expressions on days 4 and 9. The data are presented as the means ± SDs. NS means not significant; $^{*}P < 0.05$, $^{**}P < 0.01$, $^{***}P < 0.001$, and $^{****}P < 0.0001$.

of Health (No. 2022CX011) to Fulun Li, and the National Natural Science Foundation of China (No. 32371413) to Guang Yang.

Declaration of competing interest

The authors declare that there are no conflict interests of this work.

Author contribution statement

H. Z. L.: Methodology, conceptualization, investigation, data curation, formal analysis, writing original draft. M. R. C.: Methodology, conceptualization, data curation, formal analysis, writing original draft. Y. W.: Methodology, data curation, formal analysis, writing original draft. X. R. D.: Investigation, data curation,

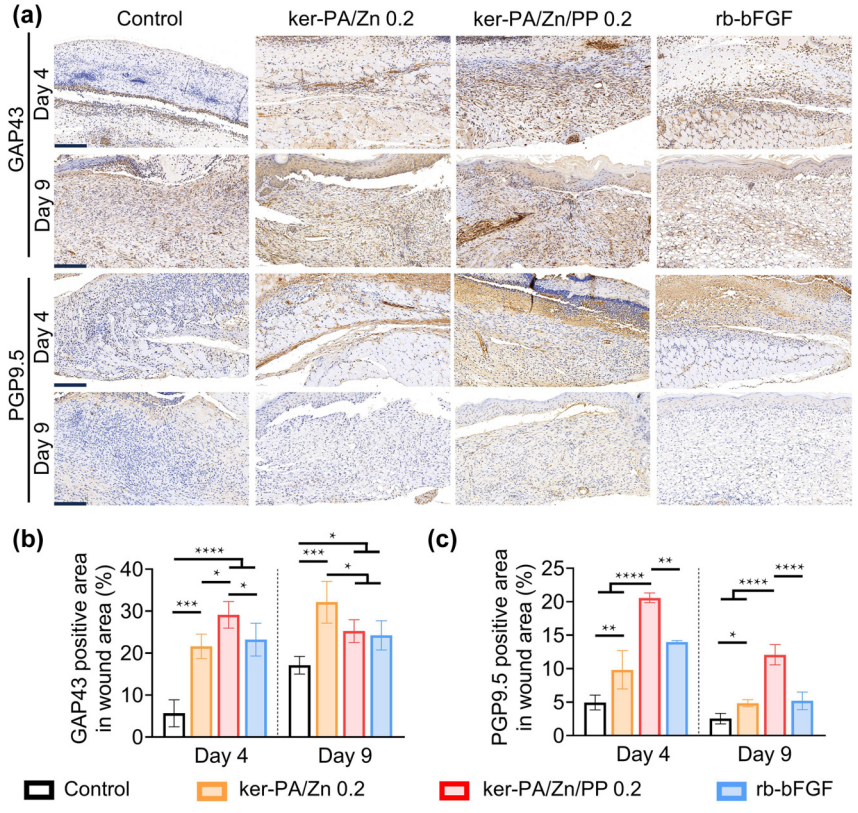

Figure 8 Effect of the ker-PA/Zn/PP 0.2 hydrogel on axon regeneration in diabetic wounds. (a) Immunohistochemical staining of GAP43 and PGP9.5 on days 4 and 9 (n = 3). Scale bars: 150 μm. (b) Quantitative analysis of GAP43. (c) Quantitative analysis of PGP9.5. The data are presented as the means ± SDs. NS means not significant; *P < 0.05, **P < 0.01, ***P < 0.001 and ****P < 0.0001.

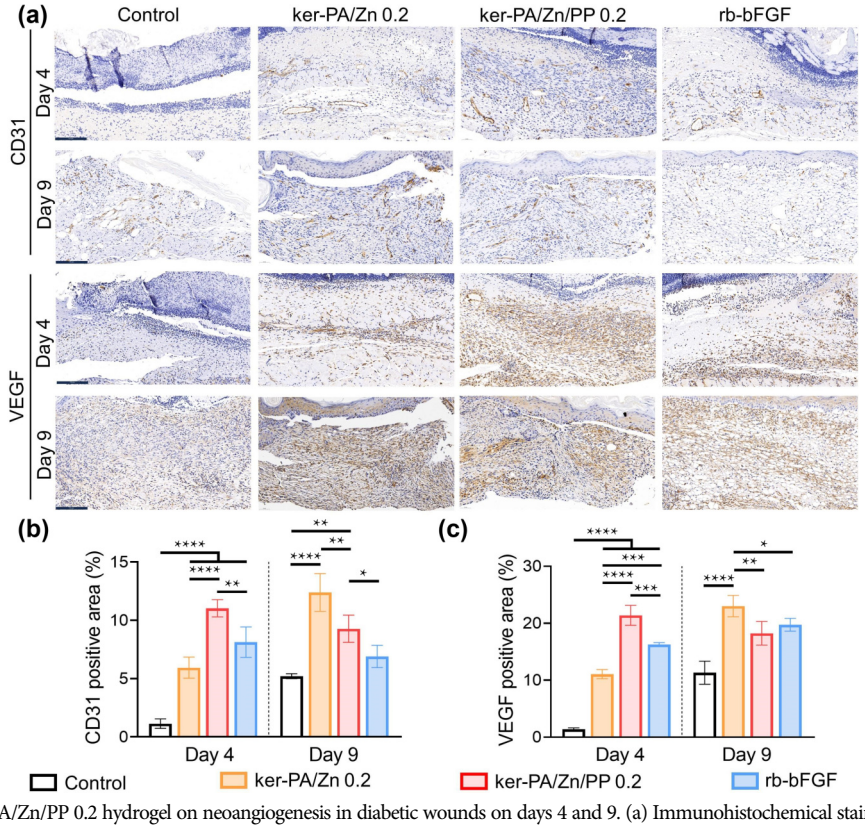

Figure 9 Effects of the ker-PA/Zn/PP 0.2 hydrogel on neoangiogenesis in diabetic wounds on days 4 and 9. (a) Immunohistochemical staining of CD31 and VEGF (n = 3). Scale bars: 150 μm. (b) Quantitative analysis of CD31 expression. (c) Quantitative analysis of VEGF. The data are presented as the means ± SDs. *P < 0.05, **P < 0.01, ***P < 0.001, and ****P < 0.0001.

writing – review & editing. X. Y. Z., Y. H. F., X. Y. G., and Y. P.: Investigation, formal analysis. J. Y. Z.: Resources, writing – review & editing. G. Y.: Conceptualization, resources, supervision, funding acquisition, writing – review & editing. F. L. L.: Conceptualization, resources, project administration, supervision, funding acquisition, writing – review & editing.

Informed consent

Not applicable.

Ethics statement

The animal experiments were approved by the Animal Care and Use Committee of Yueyang Hospital of Integrated Traditional Chinese and Western Medicine affiliated with Shanghai University of Traditional Chinese Medicine (Ethical code: YYLAC-2022-154-5).

Use of AI statement

None.

References

[1] McDermott, K.; Fang, M.; Boulton, A. J. M.; Selvin, E.; Hicks, C. W. Etiology, epidemiology, and disparities in the burden of diabetic foot ulcers. *Diabetes Care* **2023**, *46*, 209–221.

[2] Reiber, G. E.; Pecoraro, R. E.; Koepsell, T. D. Risk factors for amputation in patients with diabetes mellitus: A case-control study. *Ann. Intern. Me.* **1992**, *117*, 97–105.

[3] McNeely, M. J.; Boyko, E. J.; Ahroni, J. H.; Stensel, V. L.; Reiber, G. E.; Smith, D. G.; Pecoraro, R. F. The independent contributions of diabetic neuropathy and vasculopathy in foot ulceration: How great are the risks. *Diabetes Care* **1995**, *18*, 216–219.

[4] Reiber, G. E.; Vileikyte, L.; Boyko, E. J.; del Aguila, M.; Smith, D. G.; Lavery, L. A.; Boulton, A. J. Causal pathways for incident lower-extremity ulcers in patients with diabetes from two settings. *Diabetes Care* **1999**, *22*, 157–162.

[5] Ahmed, E. M. Hydrogel: Preparation, characterization, and applications: A review. *J. Adv. Res.* **2015**, *6*, 105–121.

[6] Liang, Y. P.; He, J. H.; Guo, B. L. Functional hydrogels as wound dressing to enhance wound healing. *ACS Nano* **2021**, *15*, 12687–12722.

[7] Ma, X. Y.; Liu, B. B.; Fan, L. M.; Liu, Y. Q.; Zhao, Y. G.; Ren, T. B.; Li, Y.; Li, Y. Y. Native and engineered exosomes for inflammatory disease. *Nano Res.* **2023**, *16*, 6991–7006.

[8] Xu, Z. J.; Liu, G. T.; Li, Q.; Wu, J. A novel hydrogel with glucose-responsive hyperglycemia regulation and antioxidant activity for enhanced diabetic wound repair. *Nano Res.* **2022**, *15*, 5305–5315.

[9] Ji, Z. X.; Wei, T.; Zhu, J. F.; Hu, J. Y.; Xiao, Z. S.; Bai, B. X.; Lv, X. Y.; Miao, Y.; Chen, M. C.; Wang, C. et al. Actively contractible and antibacterial hydrogel for accelerated wound healing. *Nano Res.* **2024**, *17*, 7394–7403.

[10] Yang, Z. X.; Zhang, Z. R.; Li, L. Y.; Jing, Z. Y.; Ma, Y. M.; Lan, T. Y.; Li, Y.; Lin, Z. D.; Fang, W. L.; Zhang, J. X. et al. Bioengineered artificial extracellular vesicles presenting PD-L1 and Gal-9 ameliorate new-onset type 1 diabetes. *Diabetes* **2024**, *73*, 1325–1335.

[11] Zheng, D. D.; Ruan, H. T.; Chen, W.; Zhang, Y. H.; Cui, W. G.; Chen, H.; Shen, H. X. Advances in extracellular vesicle functionalization strategies for tissue regeneration. *Bioact. Mater.* **2023**, *25*, 500–526.

[12] Jeffcoate, W. J.; Vileikyte, L.; Boyko, E. J.; Armstrong, D. G.; Boulton, A. J. M. Current challenges and opportunities in the prevention and management of diabetic foot ulcers. *Diabetes Care* **2018**, *41*, 645–652.

[13] Sloan, G.; Selvarajah, D.; Tesfaye, S. Pathogenesis, diagnosis and clinical management of diabetic sensorimotor peripheral neuropathy. *Nat. Rev. Endocrinol.* **2021**, *17*, 400–420.

[14] Yoo, M. C.; Chon, J.; Jung, J.; Kim, S. S.; Bae, S.; Kim, S. H.; Yeo, S. G. Potential therapeutic strategies and substances for facial nerve regeneration based on preclinical studies. *Int. J. Mol. Sci.* **2021**, *22*, 4926.

[15] Ye, W. J.; Qin, M.; Qiu, R. M.; Li, J. S. Keratin-based wound dressings: From waste to wealth. *Int. J. Biol. Macromol.* **2022**, *211*, 183–197.

[16] Chen, Y. S.; Li, Y.; Yang, X. X.; Cao, Z. J.; Nie, H. L.;Bian, Y. G.; Yang, G. Glucose-triggered *in situ* forming keratin hydrogel for the treatment of diabetic wounds. *Acta Biomate.* **2021**, *125*, 208–218.

[17] Zhang, H. J.; Ma, W. P.; Ma, H. S.; Qin, C.; Chen, J. J.; Wu, C. T. Spindle-like zinc silicate nanoparticles accelerating innervated and vascularized skin burn wound healing. *Adv. Healthc. Mater.* **2022**, *11*, 2102359.

[18] Gan, D. L.; Xing, W. S.; Jiang, L. L.; Fang, J.; Zhao, C. C.; Ren, F. Z.; Fang, L. M.; Wang, K. F.; Lu, X. Plant-inspired adhesive and tough hydrogel based on Ag-Lignin nanoparticles-triggered dynamic redox catechol chemistry. *Nat. Commun.* **2019**, *10*, 1487.

[19] Geng, H. M.; Zhong, Q. Z.; Li, J. H.; Lin, Z. X.; Cui, J. W.; Caruso, F.; Hao, J. C. Metal ion-directed functional metal-phenolic materials. *Chem. Rev.* **2022**, *122*, 11432–11473.

[20] Zhang, Q. Y.; Huang, K.; Tan, J.; Lei, X. X.; Huang, L. P.; Song, Y. T.; Li, Q. J.; Zou, C. Y.; Xie, H. Q. Metal-phenolic networks modified polyurethane as periosteum for bone regeneration. *Chin. Chem. Lett.* **2022**, *33*, 1623–1626.

[21] Sun, C. Y.; Li, W. J.; Ma, P.; Li, Y.; Zhu, Y.; Zhang, H. Y.; Adu-Frimpong, M.; Deng, W. W.; Yu, J. N.; Xu, X. M. Development of TPGS/F127/F68 mixed polymeric micelles: Enhanced oral bioavailability and hepatoprotection of syringic acid against carbon tetrachloride-induced hepatotoxicity. *Food Chem. Toxicol.* **2020**, *137*, 111126.

[22] Li, H. Y.; Wen, H. Y.; Zhang, H.; Li, J.; Cao, X.; Zhang, J. Q.; Zheng, Y. T.; Huang, S. P.; Xue, W. M.; Cai, X. J. Polymeric micelle-hydrogel composites design for biomedical applications. *Chin. Chem. Lett.* **2024**, in press, DOI: 10.1016/j.cclet.2024.110072.

[23] Huang, Y.; Gao, Q.; Li, C.; Chen, X. H.; Li, X.; He, Y.; Jin, Q.; Ji, J. Facile synthesis of Zn^{2+}-based hybrid nanoparticles as a new paradigm for the treatment of internal bacterial infections. *Adv. Funct. Mater.* **2022**, *32*, 2109011.

[24] Hua, Y. J.; Gan, Y. B.; Zhang, Y. Q.; Ouyang, B.; Tu, B.; Zhang, C. M.; Zhong, X. P.; Bao, C. Y.; Yang, Y.; Lin, Q. N. et al. Adaptable to mechanically stable hydrogels based on the dynamic covalent cross-linking of thiol-aldehyde addition. *ACS Macro Lett.* **2019**, *8*, 310–314.

[25] Cheng, C.; Singh, V.; Krishnan, A.; Kan, M.; Martinez, J. A.; Zochodne, D. W. Loss of innervation and axon plasticity accompanies impaired diabetic wound healing. *PLoS One* **2013**, *8*, e75877.

[26] Li, Q. Q.; Jiao, L.; Shao, Y. C.; Li, M. M.; Gong, M. Y.; Zhang, Y. Y.; Tan, Z. Y.; Wang, Y. Y.; Yang, X. W.; Wang, Z. G. et al. Topical GDF11 accelerates skin wound healing in both type 1 and 2 diabetic mouse models. *Biochem. Biophys. Res. Commun.* **2020**, *529*, 7–14.

[27] Theocharidis, G.; Veves, A. Autonomic nerve dysfunction and impaired diabetic wound healing: The role of neuropeptides. *Auton. Neurosci.* **2020**, *223*, 102610.

[28] Nodari, A.; Zambroni, D.; Quattrini, A.; Court, F. A.; D'Urso, A.; Recchia, A.; Tybulewicz, V. L. J.; Wrabetz, L.; Feltri, M. L. β1 integrin activates Rac1 in Schwann cells to generate radial lamellae during axonal sorting and myelination. *J. Cell Biol.* **2007**, *177*, 1063–1075.

[29] Colombelli, C.; Zambroni, D.; Occhi, S.; Wrabetz, L.; Feltri, M. L. Role of schwann cell dystroglycan in the architecture of nodes of ranvier. *J. Peripher. Nerv. Syst.* **2009**, *14*, 36.

[30] Jin, F. Z.; Dong, B. X.; Georgiou, J.; Jiang, Q. H.; Zhang, J. Y.;

Bharioke, A.; Qiu, F.; Lommel, S.; Feltri, M. L.; Wrabetz, L. et al. N-WASp is required for Schwann cell cytoskeletal dynamics, normal myelin gene expression and peripheral nerve myelination. *Development* **2011**, *138*, 1329–1337.

[31] Tello Velasquez, J.; Nazareth, L.; Quinn, R. J.; Ekberg, J. A. K.; St John, J. A. Stimulating the proliferation, migration and lamellipodia of Schwann cells using low-dose curcumin. *Neuroscience* **2016**, *324*, 140–150.

[32] Ness, J. K.; Snyder, K. M.; Tapinos, N. Lck tyrosine kinase mediates β1-integrin signalling to regulate Schwann cell migration and myelination. *Nat. Commun.* **2013**, *4*, 1912.

[33] Taveggia, C.; Feltri, M. L. Beyond wrapping: Canonical and noncanonical functions of Schwann cells. *Annu. Rev. Neurosci.* **2022**, *45*, 561–580.

[34] Zimmer, D. B.; Cornwall, E. H.; Landar, A.; Song, W. The S100 protein family: History, function, and expression. *Brain Res. Bull.* **1995**, *37*, 417–429.

[35] Tian, T.; Yu, Z. H.; Zhang, N. L.; Chang, Y. W.; Zhang, Y. Q.; Zhang, L. P.; Zhou, S.; Zhang, C. L.; Feng, G. Y.; Huang, F. Modified acellular nerve-delivering PMSCs improve functional recovery in rats after complete spinal cord transection. *Biomater. Sci.* **2017**, *5*, 2480–2492.

[36] Li, X.; He, N.; Li, X. J.; Wang, X.; Zhan, L.; Yuan, W. E.; Song, J. L.; Ouyang, Y. M. Graphdiyne-loaded polycaprolactone nanofiber scaffold for peripheral nerve regeneration. *J. Colloid Interface Sci.* **2023**, *646*, 399–412.

[37] Wang, C. G.; Wang, Q. Q.; Gao, W. D.; Zhang, Z. J.; Lou, Y. T.; Jin, H. M.; Chen, X. F.; Lei, B.; Xu, H. Z.; Mao, C. Highly efficient local delivery of endothelial progenitor cells significantly potentiates angiogenesis and full-thickness wound healing. *Acta Biomater.* **2018**, *69*, 156–169.

[38] Zhang, Z. W. B.; Li, W. B.; Chang, D.; Wei, Z. Q.; Wang, E. D.; Yu, J.; Xu, Y. Z.; Que, Y. M.; Chen, Y. M.; Fan, C.; et al. A combination therapy for androgenic alopecia based on quercetin and zinc/copper dual-doped mesoporous silica nanocomposite microneedle patch. *Bioact. Mater.* **2023**, *24*, 81–95.

[39] Hu, S. Q.; Li, Z. H.; Lutz, H.; Huang, K.; Su, T.; Cores, J.; Dinh, P. U. C.; Cheng, K. Dermal exosomes containing miR-218-5p promote hair regeneration by regulating β-catenin signaling. *Sci. Adv.* **2020**, *6*, eaba1685.

[40] Feliú, A.; del Río, I. B.; Carrillo-Salinas, F. J.; Hernández-Torres, G.; Mestre, L.; Puente, N.; Ortega-Gutiérrez, S.; Lopez-Rodríguez, M. L.; Grandes, P.; Mecha, M. et al. 2-arachidonoylglycerol reduces proteoglycans and enhances remyelination in a progressive model of demyelination. *J. Neurosci.* **2017**, *37*, 8385–8398.

[41] Fantini, F.; Johansson, O. Expression of growth-associated protein 43 and nerve growth factor receptor in human skin: A comparative immunohistochemical investigation. *J. Invest. Dermatol.* **1992**, *99*, 734–742.

[42] Pradhan, L.; Nabzdyk, C.; Andersen, N. D.; LoGerfo, F. W.; Veves, A. Inflammation and neuropeptides: The connection in diabetic wound healing. *Expert Rev. Mol. Med.* **2009**, *11*, e2.

[43] Boyette-Davis, J.; Xin, W.; Zhang, H.; Dougherty, P. M. Intraepidermal nerve fiber loss corresponds to the development of taxol-induced hyperalgesia and can be prevented by treatment with minocycline. *Pain* **2011**, *152*, 308–313.

[44] Xuan, Y. W.; Li, L.; Yin, X. L.; He, D. M.; Li, S. Y.; Zhang, C. P.; Yin, Y.; Xu, W. L.; Zhang, Z. Bredigite-based bioactive nerve guidance conduit for pro-healing macrophage polarization and peripheral nerve regeneration. *Adv. Healthc. Mater.* **2024**, *13*, 2302994.

[45] Okonkwo, U. A.; DiPietro, L. A. Diabetes and wound angiogenesis. *Int. J. Mol. Sci.* **2017**, *18*, 1419.

[46] Nowak, N. C.; Menichella, D. M.; Miller, R.; Paller, A. S. Cutaneous innervation in impaired diabetic wound healing. *Transl. Res.* **2021**, *236*, 87–108.